ARTICLE

Relationship of Surface Hydrophilicity, Charge, and Roughness of PET Foils Stimulated by Incipient Alkaline Hydrolysis

Jiří Škvarla,*,† Thomas Luxbacher,‡ Martin Nagy,† and Martin Sisol†

Institute of Montaneous Sciences and Environmental Protection, Center of Primary and Secondary Raw Materials Processing, Technical University in Košice, Park Komenského 19, 043 84 Košice, Slovak Republic, and Anton Paar GmbH, Anto Paar Strasse 20, A-8054, Austria

ABSTRACT An enhancement of wettability of PET foils pretreated hydrolytically by immersing in mild alkaline (NaOH) solutions has been documented by a descending sigmoidal dependence between the interfacial free energy γ_{SL} of the PET/water interface and the concentration of NaOH solution c_{NaOH}. An increase in temperature of the NaOH solution below the glass-transition temperature of PET further promotes the hydrophilicity, resulting in a proportional shift of the γ_{SL} vs c_{NaOH} dependence. The limiting hydrophilicity of PET is thermodynamically predicted to occur at $\gamma_{SL} \rightarrow 0$, corresponding to the advancing water contact angle $\theta_a \approx 50°$ (for 6% NaOH and 60 °C). The surface roughness due to the partial hydrolytic degradation as well as the weight loss (dissolution) of PET are found to reach a maximum value just when the latter dependence goes through its inflection. Assuming a general parallelism between the interfacial free energy and the dissolution kinetics, we propose the hydrolytically stimulated formation and growth of pits on the PET surface to cause the initial acceleration as well as subsequent retardation of dissolution as c_{NaOH} increases, leading to the S-shaped γ_{SL} vs c_{NaOH} dependence with the inflection for a specific c_{NaOH}. Moreover, the zeta potential measured by the streaming current method also attains a maximum at the same specific concentration of NaOH. It would indicate that the largest amount of electric charges is populated via polar carboxyl and hydroxyl groups created by chemical scissions of PET polymer chains when a change in the dissolution rate increases to the utmost. In such a way, partial hydrolysis restricted to the uppermost part of moderately hydrophobic surface of solid PET allowed us to better understand the intermingled role of thermodynamic and physical aspects in surface wettability itself.

KEYWORDS: PET • hydrolysis • wettability • surface roughness • interfacial free energy • contact angle • alkaline degradation • dissolution

1. INTRODUCTION

The physicochemical process of flotation is often adopted to selectively separate various materials including solid polymers basing on a difference in their surface wettabilities. Nevertheless, since many polymers, including PET and PVC, are similar with respect to the relatively strong surface hydrophobicity (floatability), the selective flotation separation of their mixtures is not possible without a significant and yet selective hydrophilization pretreatment.

To make the surface of polymers selectively water-wettable and thus nonfloatable, researchers consider applying wetting agents (1−3) or physical treatments such as flame (4) or ozonation (5−9). Moreover, to improve not only wettability but also the printability, biocompatibility, conductivity, permeability, adhesivity, etc., of the PET surface, researchers have studied its modification by plasma (10−14) and photocatalytic oxidation (15) even more extensively. However, some chemical treatments seem to be viable as well. Indeed, it has been found that the surface of PET can be hydrophilized (selectively in its mixture with PVC, leaving the PVC surface almost untouched) by immersing in a NaOH solution heated for a short time period at the atmospheric pressure, resulting in the suppression of PET flotation (16, 17).

In fact, alkaline, neutral, and acidic hydrolysis is the only method of chemical depolymerization recycling of PET that provides terephthalic acid (TPA) and monoethylene glycol (EG) monomers. When reacting TPA with EG (polyesterification), a regenerated PET can be thus produced (18−25). Nevertheless, its main disadvantage is that it occurs at relatively high temperatures (200−250 °C) and pressures (1.4−2 MPa) and a purification of TPA is necessary (26). If the chemical depolymerization is carried out in milder experimental conditions and temperatures below 100 °C, a phase-transfer catalyst is needed (27, 28). The argument is that although the alkaline hydrolysis reaction is very fast in the molten state of PET, it slows down significantly below its melting range (245−265 °C), becoming a very complex process limited by various physical factors such as diffusion, crystallinity, morphology, chain mobility, permeability, etc.

Hydrolysis of solid PET is even less prominent at temperatures below its glass-transition temperature ($T_g \approx 85$ °C) (29−32). It is, however, still effective enough to render PET hydrophilic to such an extent that it becomes nonfloatable, as already mentioned. Simultaneously, as follows for example from experiments on polyester fibers and fabrics in

* Corresponding author. Tel: +421 (55) 602 2962. Fax: +421 (55) 602 2957. E-mail: jiri.skvarla@tuke.sk.

Received for review April 27, 2010 and accepted June 17, 2010

† Technical University in Košice.

‡ Anton Paar GmbH.

DOI: 10.1021/am100368v

Published on Web 06/28/2010

textile assemblies pretreated with 10% sodium hydroxide solution at 60 °C, not only an increase in the number of polymer hydrophilic groups resulting from chain scissions on the planar surface (chemical alteration) but also in pits formed and grown within the surface (physical alteration) may be at the origin of the enhanced wettability of PET (33−36).

Hence, it can be expected from the above that hydrophilicity (polarity) of PET stimulated by partial alkaline hydrolysis reaction will be influenced by the mechanism and rate (extent) of the dissolution of reaction products whereby the outerrmost PET surface is deteriorated. Moreover, the impact of surface dissolution and/or soprtion/crystallization of dissolution products, represented by various surface roughness parameters, on parameters used obviously to evaluate the surface wettability (e.g., the contact angle) is still not understood satisfactorily in general. (This is apparently a result of a wide range of heterogenities accompanying chemical reactions at interfaces).

Therefore, the aim of this study is 2-fold. First, hydrophilicity of PET foils will be determined by contact angle goniometry in order to evaluate a short-time impact of basic factors of hydrolytic degradation (temperature and concentration of the NaOH pretreatment solution), on it. Subsequently, the coresponding interfacial free energy at the PET/water interface will be determined from the contact angle data. Second, morphology of these foils will be evaluated by scanning electron (SEM) and atomic force microscopy (AFM) with an intention of assessing the role of surface roughness in the hydrolytically induced changes of hydrophilicity and interfacial tension. Additionally, the streaming current measurements of PET surface charge density will be carried out in attempt to better describe the latter changes.

2. EXPERIMENTAL SECTION

2.1. Samples and Their Pretreatment. Technical PET foils with the thickness of 0.2 mm, cut from postconsumer plastic bottles were used throughout the study. The foil samples with the size of ca. 20 × 20 mm^2 and without any preliminary cleaning procedure were immersed in a series of aqueous sodium hydroxide solutions with the concentration of 0, 2, 4, and 6 wt % (corresponding to 0, 0.51, 1.04, and 1.6 M, respectively) and temperatures (20, 40, 60, and 80 °C) and stirred continuously for the period of 20 min. Then, the NaOH-treated samples were taken out of the bath, washed with a copious supply of distilled water to remove the remaining NaOH, and air-dried at 30 °C. The individual samples are denoted as PETc/T throughout this study, with c and T being the NaOH concentration in wt % and temperature in °C of the pretreatment solution, respectively.

2.2. SEM and AFM. The scanning electron microscope Quanta FEI 400 with the accelerating voltage of 30 kV and the detector of secondary electrons was used to image the PET surface topography at the magnification of 10,000× to 40,000×. The Nanosurf EasyScan Flex AFM in the dynamic mode with the NCLR cantilever was used to visualize the nanotexture and to measure the mean nanoroughness of the PET surface at scan sizes of 2, 5, and 30 μm. The mean roughness parameter S_a is defined as the arithmetic average of deviation from a median plane

$$S_a = \frac{\int_{y=0}^{y_r}\int_{x=0}^{x_r} |z(x,y) - \mu| \mathrm{d}x\mathrm{d}y}{x_r y_r} \quad (1)$$

with

$$\mu = \frac{\int_{y=0}^{y_r}\int_{x=0}^{x_r} z(x,y) \mathrm{d}x\mathrm{d}y}{x_r y_r} \quad (2)$$

where an x, y, z coordinate system is taken as the reference for the measurement, with the origin ($x = 0, y = 0$) coincident with the beginning of the scan; z is the vertical elevation of the surface measured by the AFM in the position (x, y); x_r and y_r are the measured scan sizes, respectively, in the x and y direction; μ is the mean value. Samples of untreated and treated PET were analyzed on randomly selected positions all over the sample surface.

2.3. Gravimetry. The degradation C in the course of hydrolytic reaction was determined from the polymer weight loss or gain at room temperature using the following equation:

$$C(\%) = \frac{m - m_0}{m_0} 100 \quad (3)$$

where m_0 and m refer, respectively, to the initial dry weight of (untreated) PET foils and the weight of the same PET foils periodically removed and dried at 30 °C after immersing them in NaOH solutions of different concentrations at ambient temperature at increasing period of time.

2.4. Electrokinetics (Streaming Current). The streaming current measurements were performed with the Anton-Paar electrokinetic analyzer SurPASS using the Clamping Cell that allows flattening of bent PET samples. For each measurement, a pair of PET foil sample was separated by a spacer introducing a gap of approximately 100 μm. A 1 mM KCl solution was used as the background electrolyte and its pH was adjusted with 0.1 M HCl and 0.1 M NaOH, respectively. The dependence of streaming current on the applied differential pressure was strictly linear with a coefficient of linear regression better than $R^2 = 0.99$. Similarly, a linear dependence of the volume flow rate vs differential pressure was detected (with the same slope irrespective of pH of the KCl solution), indicating a laminar flow behavior. The slope of the latter dependence was used to calculate the exact dimensions of the streaming channel (the gap between the planar surfaces). The ζ-potential was calculated acording to the equation

$$\zeta = \frac{\mathrm{d}I}{\mathrm{d}p} \frac{\eta}{\varepsilon\varepsilon_0} \frac{L}{A} \quad (4)$$

where dI/dp is the slope of the streaming current vs the differential pressure, η is the electrolyte solution viscosity, ε_0 is the dielectric coefficient of the vacuum, ε is the dielectric coefficient of the electrolyte solution, and L and A are the length and the cross-section of the streaming channel, respectively.

The results of streaming current measurements using different measuring cells (Adjustable Gap Cell and CLAMP) differed slightly in the alkaline region but a satisfying agreement was seen in the pH range from 4 to 7 (not shown here).

2.5. Contact Angle Goniometry. A sessile drop technique was used to measure the static advancing θ_a and the receding contact angle θ_r of small (∼3 μL) water drops (whose front

progressed and receded, respectively) on the PET foil samples in air by the Krüss EasyDrop Contact Angle Measuring System, allowing a high-precision dosing, positioning, and imaging of the liquids drops. The evaluation of digitized video images and the calculation of contact angles were made with the Drop Shape Analysis (DSA1) software. For each surface, contact angles were measured on both sides of at least 10 randomly positioned drops and averaged. The scatter in the contact angle values did not exceed 3°. The water contact angle hysteresis (CAH) was determined as

$$\Delta\theta = \theta_a - \theta_r \tag{5}$$

To evaluate the surface free energy γ_S of PET samples, we adopted the Young−Dupré equation in the form derived from the Lifshitz−van der Waals/Lewis acid−base (LW-AB) surface thermodynamics theory, also known as the van Oss−Chaudhury−Good (VCG) model

$$\gamma_L(\cos\theta + 1) = 2\sqrt{\gamma_S^{LW}\gamma_L^{LW}} + 2\sqrt{\gamma_S^{+}\gamma_L^{-}} + 2\sqrt{\gamma_S^{-}\gamma_L^{+}} \tag{6}$$

As follows from eq 6, the LW component and the electron-donor and electron-acceptor parameters (providing the Lewis AB component) of a solid's surface energy, i.e., γ_S^{LW}, γ_S^{+}, and γ_S^{-} ($\gamma_S^{AB} = \sqrt{\gamma_S^{+}\gamma_S^{-}}$), respectively, are combined with their counterparts of a test liquid, i.e., γ_L^{LW}, γ_L^{+}, and γ_L^{-}, according to the simple Berthelot geometric mean rule. Thus, the surface energy parameters and components of PET can be calculated when the counterparts of three different test liquids (of which two should be polar) are known and contact angles of their drops are measured on the PET surface and inserted in eq 6. It means that three eq 6s must be solved as a set of linear equations. Accordingly, advancing contact angles of two triplets of frequently used test liquids were measured, namely α-bromonaphthalene-glycerol−water (BN-GL-W) and diodomethane-glycerol−water (DM-GL-W).

The PET/water interfacial free energy or tension γ_{SL} was then calculated from γ_S by using the Young equation

$$\gamma_{SL} = \gamma_S - \gamma_L\cos\theta_L \tag{7}$$

in which γ_L and θ_L is the surface tension and advancing contact angle of water, respectively.

It should be mentioned that the VCG wetting theory allows for negative values of interface tension, as follows from the following definition

$$\gamma_{SL} = (\sqrt{\gamma_S^{LW}} - \sqrt{\gamma_L^{LW}})^2 + 2(\sqrt{\gamma_S^{+}\gamma_S^{-}} + \sqrt{\gamma_L^{+}\gamma_L^{-}}) - (\sqrt{\gamma_S^{+}\gamma_L^{-}} - \sqrt{\gamma_S^{-}\gamma_L^{+}}) \tag{8}$$

3. RESULTS AND DISCUSSION

3.1. Topography. Figure 1 presents the SEM images of a PET foil surface untreated (a) and pretreated under relatively most drastic conditions, i.e. in 6% NaOH solution at 60 °C, PET6/60 (b, c). It can be seen that the untreated surface looks very smooth, whereas the pretreated surface is rougher because of the partial hydrolysis. Moreover, on the pretreated surface, small pits are distinguishable.

Figure 2 complements the above SEM images, displaying the 2 × 2 μm AFM scans of PET surface untreated (a) and pretreated in a series of less drastic conditions, i.e., in 2% NaOH at 40 °C (PET2/40, b), 4% NaOH at 40 °C (PET4/40, c), and 2% NaOH at 60 °C (PET2/60, d). Sporadic and low elevations are detected only on the very smooth and homogeneous surface of untreated PET. The conditioning results in a broken relief of the PET2/40 surface with hills, depressions, and occasional small but deep cavities (pits). The same features (bumps and holes) can be observed on the scan taken for the PET4/40 sample. The PET2/60 sample manifests well-identifiable islands of rounded shape and different diameter (up to ca. 0.8 μm), encircled with an array of pits. Referring to the SEM and AFM images (Figure 1 and 2), lateral heterogeneities of PET surfaces pretreated in the NaOH solution are apparent. The difference between the highest and lowest points is evaluated to be, in the above order of samples, 2−3, 5−7, 7−10, and 10−12 nm.

3.2. Roughness. The mean surface (area) parameter S_a (eqs 1 and 2) quantifying roughness of the PET surface due to the NaOH-induced degradation by analyzing individual AFM scans of different sizes is displayed in Figure 3. It can be seen that the surface roughness increases within a nanometric scale with the increasing concentration and temperature of pretreatment NaOH solution, indicating the surface had become eroded increasingly by hydrolysis.

For the 2 × 2 μm^2 scans, S_a increases from 0.69 nm on the untreated PET to 2.37 and 2.31 nm on the PET6/40 and PET2/60, respectively. For 5 × 5 μm scans, S_a increases, respectively, from 0.92 nm to 2.74 and 3.25 nm. Interestingly, the surface roughness for PET4/40 is quite low (S_a = 1.00 and 1.04 nm for 2 × 2 μm and 5 × 5 μm scans, respectively). Nevertheless, the roughness seems to be at a relative maximum (S_a = 2.80 nm) for the same sample for the 40 °C series when the scan size is 30 × 30 μm.

It is known that roughness parameters increase with the scan size. Apparently, S_a for the 5 × 5 μm^2 scans really lies between that for the 2 × 2 μm^2 and the 30 × 30 μm^2 scans, with the only exception being PET6/40. We ascribe this to scratches present on the PET surfaces. More reliable results would be obtained when basing S_a on calculations from multiple (averaged) rather than individual scans. However, in principle, we can consider the largest scans (30 × 30 μm^2) as the most reliable ones. If so, the surface roughness of PET is predicted to increase with the NaOH concentration increasing up to 4% and decreases above this concentration.

3.3. Degradation. Figure 4 reveals that a PET foil, after its immersion in the distilled water at room temperature for only 2 h, becomes heavier than before the immersion so that the degradation C (= 0.0135%) after eq 3 is positive. This small weight gain of the foil is however replaced with a small weight loss (C = −0.026%) after 10 h immersion. This indicates that the initial sorption of water molecules not removed from the PET surface after drying must be overcome with the PET dissolution after elapsing a time (C = 0 at ca. 4 h). Both the weight gain and the subsequent weight loss increase continuously with the ad-

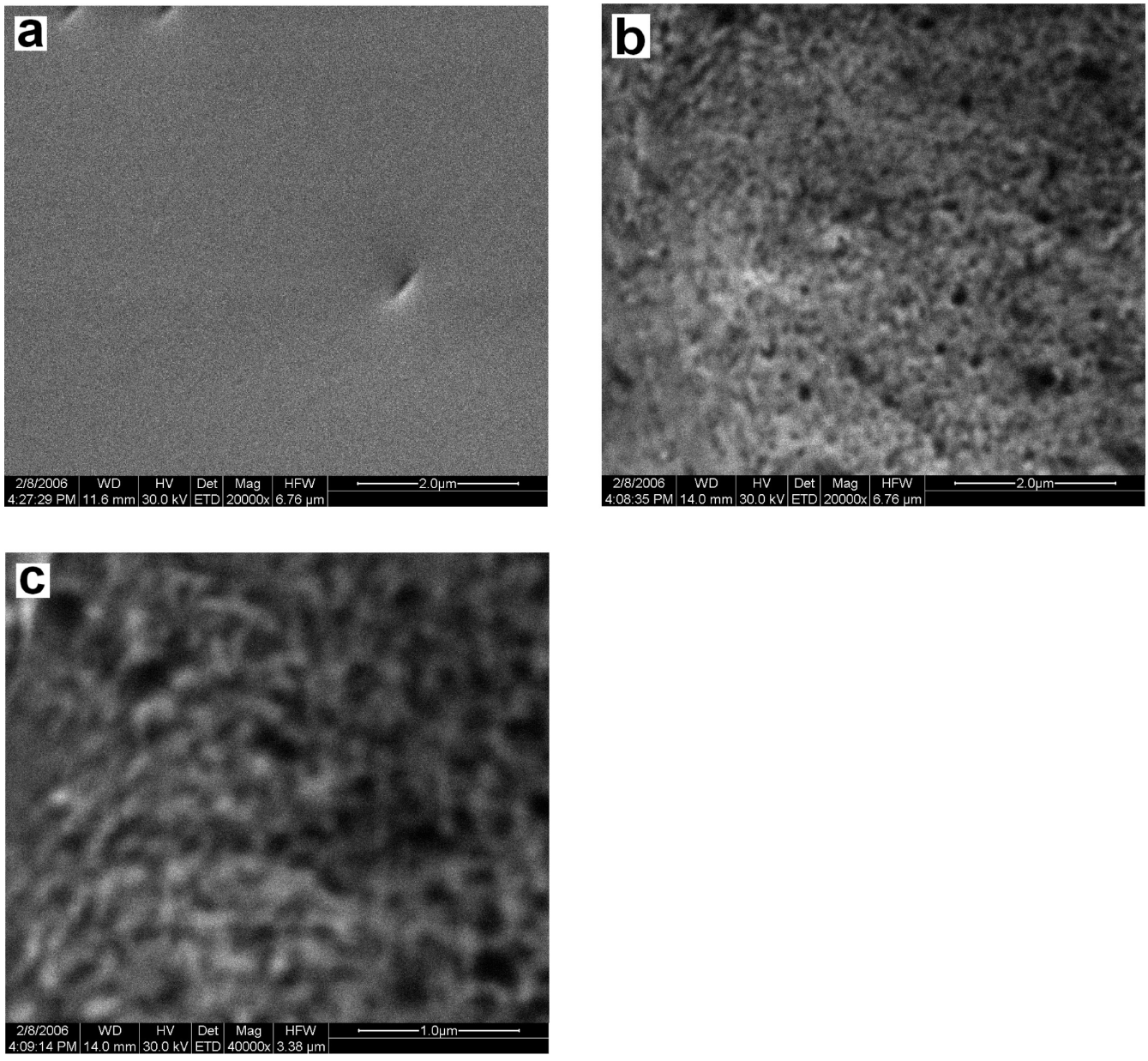

FIGURE 1. SEM images of (a) untreated PET and (b, c) NaOH-modified PET6/60. Magnification: 20 000× (a, b) and 40 000× (c).

dition of NaOH in the solution up to 6% when C attains values of 0.2347 and −0.1252% after 2 and 10 h, respectively. In 8% NaOH, the weight gain (0.0619%) after 2 h as well as the weight loss (−0.101%) after 10 h diminished.

A general mechanism of the hydrolytic reaction at the PET surface in acidic, neutral, and alkaline conditions is proposed as follows (34, 35). In acidic and neutral aqueous solutions, the polymer in-chain oxygen atom of the ester group is protonated, and, being followed by a reaction with water, equivalent amounts of hydroxyl and carboxyl end groups and chain fragments are produced; in alkaline solutions, the hydroxide anion attacks the carboxyl oxygen atom producing equivalent amounts of hydroxyl and carboxyl end groups.

Therefore, the rate of hydrolysis of PET increases dramatically in the NaOH solutions resulting in its progressive degradation, as confirmed in Figure 4. When assuming sorption and dissolution to run simultaneously from the beginning of PET immersion in NaOH solutions, it can be predicted that there is a maximum in the PET dissolution in 6% NaOH after 20 min, even though a (maximum) sorption of water would only be expectable for such hydrolysis (Figure 4d).

The results of degradation experiments (Figure 4) can be better understood by following the sorption kinetics of water into the PET structure. It was found earlier using a gravimetric method (37) that the kinetics of water sorption in amorphous PET films at 20 °C follows the Fickian diffusion law. The sorption rate w/w_{eq} is defined as a function of dimensionless time parameter $\tau = Dt/l^2$:

$$w/w_{eq} = 4(\tau/\pi)^{1/2} \text{ for } \tau \leq 0.0492 \qquad (9a)$$

$$w/w_{eq} = 1 - \frac{8}{\pi^2}\sum_{0}^{\infty}\frac{1}{(2n+1)^2}\exp[-(2n+1)^2\pi^2\tau] \quad \text{for } \tau > 0.0492 \quad (9b)$$

where w_{eq} is the water content at equilibrium, $D \approx 4.5 \times 10^{-5}$ m^2 s^{-1} is the apparent water diffusion coefficient for different kinds of PET at ~25 °C, and l is the film thickness. The Fickian water sorption has also been confirmed without significant swelling for a crystallinity range 4 − 25% (38, 39).

Considering the validity of eq 9a for our 0.2 mm thick PET foils, the sorption rate is approximated to be 0.64 and 0.97 at the dimensionless time $\tau = 0.081$ ($t = 2$ h) and 0.405 ($t = 10$ h), respectively. It would mean that 65% of water is sorbed after 2 h whereas the sorption process will be almost complete after 10 h. Initially, the sorption increases linearly with $\sqrt{\tau}$ according to eq 9ba but starts to relatively slow down when eq 9ab becomes operative, i.e. after elapsing 1.2 h ($\tau = 0.0492$) (an FTIR-ATR study documented that the infrared spectrum of water sorbed in PET at 25 °C varies with time especially up to only ca. 150 min, reflecting hydrogen-bonding changes within water molecule "clusters" inside the polymer matrix (40)).

It follows from the above that at the weight gain−loss transition, detected by our degradation experiments to be at $t \approx 4$ h (Figure 4), dissolution of PET polymers starts to dominate the water sorption when (and because) the sorption process is decelerated appreciably but not entirely terminated.

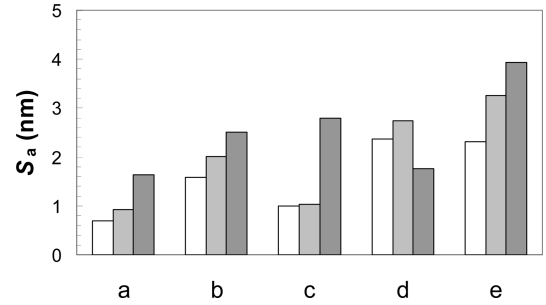

FIGURE 3. Mean surface parameter S_a of (a) untreated PET and (b) NaOH-modified PET2/40, (c) PET4/40, (d) PET6/40, and (e) PET2/60. The scan sizes were 2 × 2, 5 × 5, and 30 × 30 μm^2 (left, middle, and right columns, respectively).

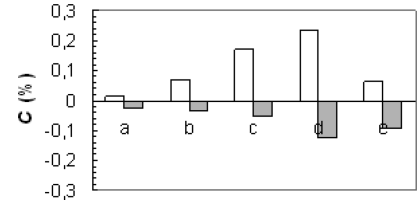

FIGURE 4. Degradation C of PET immersed in (a) water, (b) 2% NaOH, (c) 4% (NaOH), (d) 6% NaOH, and (e) 8% NaOH for 2 and 10 h at ambient temperature (left and right columns, respectively).

3.4. Zeta Potential. In comparison with more polar polymers, PET does not tend to swell extensively in aqueous

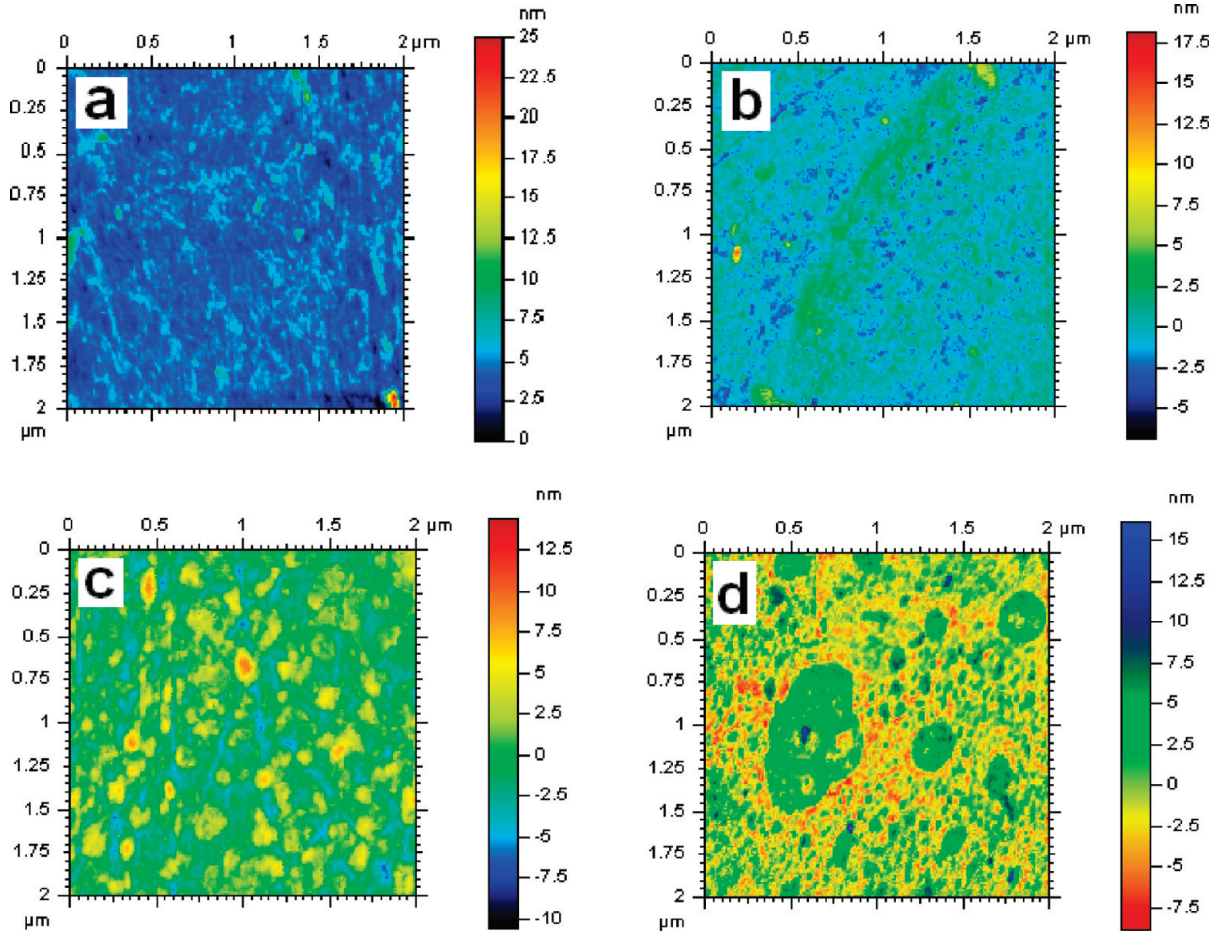

FIGURE 2. AFM images of (a) untreated PET and (b) NaOH-modified PET2/40, (c) PET4/40, and (d) PET2/60. The scan size is 2 × 2 μm^2.

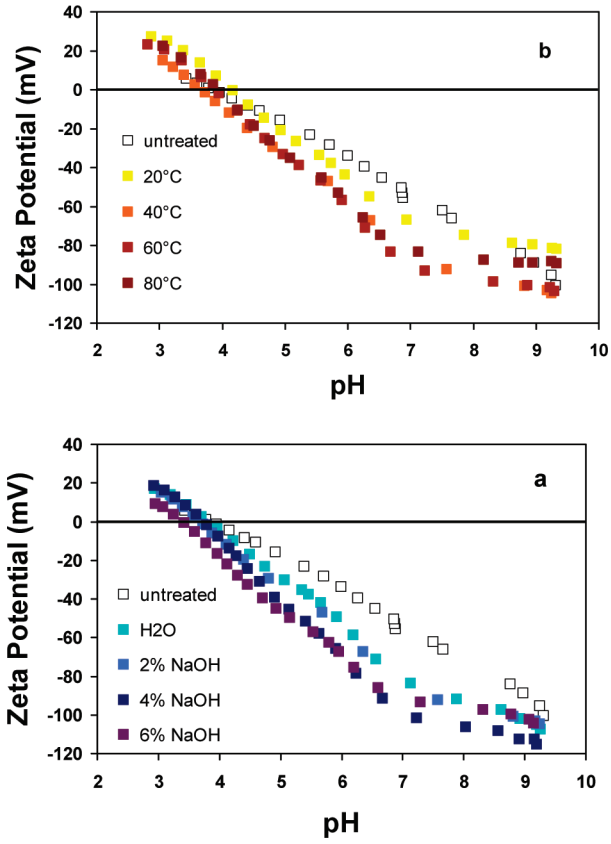

FIGURE 5. ζ vs pH dependences for PET foils pretreated in solutions of various (a) NaOH concentration (at 40 °C) and (b) temperature (2% NaOH).

solutions (41), as shown by a low water vapor adsorption at 65% rel. humidity (0.3%) and a relatively high ζ-potential of PET fibers in water, not changing within a relatively short time period (42). If swelling of polymeric chains should be the only effect at the PET surface, it would cause a time-dependent shift of the shear plane from the "dry" surface into the water phase, leading to a reduction in the negative ζ (43). Actually, a 7.4 mV decrease in the initial ζ of PET fibers at the first contact with distilled water to the final ζ approached asymptotically at infinite time was detected electrokinetically (44), meaning a relatively weak effect of long-term swelling of PET at an ambient temperature.

Figure 5 shows how the hydrolysis of PET foils is reflected in their ζ potential measured in 1 mM KCl solutions of varying pH.

Apparently, the ζ vs pH dependences are double-linear, with a higher and lower rate of increase in ζ below and above pH ∼7, respectively. More importantly, these dependences are found to shift toward more negative values of ζ potential when the concentration (Figure 5a) or temperature (Figure 5b) of the pretreatment NaOH solution had increased. The mere pretreatment in water at 40 °C (PET0/40) eventuates in more negative ζ values; Figure 5a shows that at the break point (pH 7) the absolute value of ζ increases from −53 mV for untreated PET to −80 mV for PET0/40. However, the ζ potential rises continually on samples pretreated in solutions with concentrations of up to only 4%, providing ζ as high as −100 mV for PET4/40, with a further increase in the NaOH concentration of the pretreatment solution resulting in the reverse trend (i.e., a decrease in ζ to −90 mV for PET6/40, at pH 7). Figure 5b shows an analogous effect due to the increasing temperature of 2% NaOH solution. The maximum ζ value observed for PET2/60 or PET2/80 (ca. −100 mV) is roughly equivalent to the limiting value of PET4/40.

Moreover, Figure 5a reveals that there is a seemingly uneven minor variation in the pH at which ζ becomes zero, i.e., the isoelectric point (IEP). So, pH_{IEP} is 3.87, 3.7, 3.78, and 3.4 for PET0/40, 2/40, 4/40, and 6/40, respectively. For the series of PET surfaces pretreated in different NaOH solutions, the trend in the zeta potential changes at higher pHs is therefore not the same as that in pH_{IEP}.

At first sight, it can be expected that the initial increase in the ζ-potential with the increasing concentration of NaOH pretreatment solution at 40 °C (Figure 5a) is caused by an increasing formation of acidic (hydrophilic) functional groups at the PET surface as a consequence of progressive alkaline hydrolysis. Consequently, the apparent discontinuation in the ζ value increase noticed for PET4/40 could be explained by an enhanced dissolution of these charged polar groups from the surface while pretreated in more concentrated NaOH solutions. Analogously, the ζ-potential of LDPE polymer was found to change with an increasing time of the UV irradiation (photosulfonation) modification but then remained constant due to an increasing solubility of components with sulfonic acid groups from the irradiation-induced network at the modified LDPE surface (45).

However, more detailed electrokinetic theories (46−49) taking into account various surface inhomogeneities could interpret the obtained changes in the ζ potential (which is not a measurable but derived quantity) at the PET surface, possibly without the need of invoking the idea of the generation and dissolution equilibrium of charged groups. In fact, both factors that determine electrokinetic phenomena, i.e., the hydrodynamic flow and the electric field pattern, are influenced by the morphology of the solid/liquid interface in a complicated way. According to these theories, the electrophoretic mobility of surfaces with a charged structured layer exerting a negligible friction on water should be higher than that for a smooth surface carrying the same amount of charge. It is also known that small electrokinetic potentials are measured on solid surfaces covered by hydrodynamically not very permeable but highly (titrable) charged gel-like layers of the same material, formed when water penetrates and/or interacts with this surface.

Apparently, the resulting increase in ζ of PET2/40 and 4/40, as compared with that of PET0/40, may be associated not only with the hydrolytically stimulated accumulation of additional electric charge on otherwise ideally smooth PET surface but also with a gradual exposition of the (invariable) "residual" electric charges spread through an increasingly thick swelling polymer layer permeable enough for water molecules. In the same way, the cessation of the ζ increase observed for PET6/40 might still reflect a presence of this layer that continues to develop into a more extensive and/

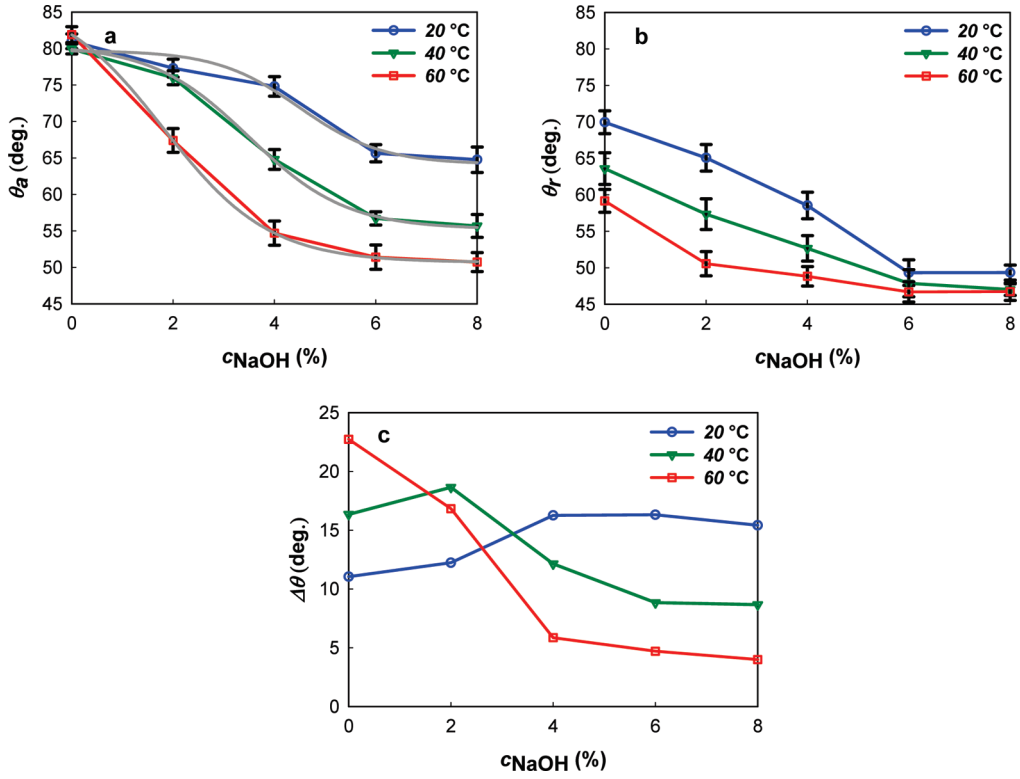

FIGURE 6. (a) Advancing θ_a and (b) receding θ_r contact angle and (c) their hysteresis $\Delta\theta$ of water drops on PET as a function of concentration of the NaOH pretreatment solution.

or dense structure, preventing water molecules to penetrate inside, so that a lower amount of charge is "felt" electrokinetically.

Nevertheless, it should be recalled that the hydrolytic degradation−dissolution is undoubtedly an ongoing process at 40 °C, as evidenced by the PET surface with pits, at least for foils pretreated in NaOH solutions, see the AFM images in Figure 2b−d. The pits (with unchanged surface chemistry) covering the surface of PETs pretreated at 40 °C however do not seem to influence the obtained ζ potential data. The argument is that, within limits of the simple electrokinetic model introduced by Hayes (50), an increase in both the size and number of depressions on an initially smooth surface leads to a reduction in ζ. Schnitzer and Ripperger (51) indeed found ζ values on mechanically roughened polyester plates to decrease in line with Hayes's model, with the pH_{IEP} to be invariant (∼3.9) because the plates' surface chemistry was the same. Naturally, this contradicts qualitatively what has been measured on PET surfaces etched by increasingly concentrated NaOH solutions (Figure 5).

Apparently, when considering the pits to be the only or main cause of the detected trend in the ζ potential, their surface chemistry should have been changing, probably through a variation in the relative proportion of newly formed and dissolved functional groups, as previously mentioned. It is worth mentioning that a swelling layer could still exist at the PET surface immersed in water and NaOH solutions at 40 °C due to the ingress of water molecules into the surface (pits), connected with a disruption of polymer−polymer interactions. Indeed, PET films were found to exhibit a softening (swelling) within 10 min of exposure to water at 75 °C (52) but experiments at temperatures around 30 °C (37−40) apparently do not support this idea. Because ζ values in this study were calculated from the streaming current, they are not misrepresented by the surface conductivity (53, 54). However, because a surface layer may provide an extra surface conductivity much higher than a respective plane Gouy−Chapman double-layer, a comparison of ζ potentials obtained from streaming currents and potentials in solutions of low ionic strengths can better resolve the above problem.

3.5. Wettability. Figure 6 gives a picture of the effect of NaOH pretreatment on the advancing θ_a (a) and receding θ_r (b) water contact angle, as well as to their hysteresis $\Delta\theta$ (c) on PET foil samples. The values of both θ_a and θ_r measured on untreated PET (in common with PET0/20), i.e., ∼81 and ∼70°, respectively, agree well with those measured by other authors on virgin PETs. θ_a has been published to be 76.5° on PET plates cleaned in a detergent solution, rinsed several times with distilled water and finally treated in an ultrasonic bath (55, 56). A slightly higher value (79.09°) was presented for exceedingly smooth PET films (American Hoechst Corp.) cleaned with methanol and acetone before use (57). $\theta_a = 81°$ (58) is closest to our θ_a but values as high as 85° have also been found in the literature for PET fibers washed in ethanol followed by twice rinses in distilled water and then dried at 40 °C (59).

As Figure 6 shows, neutral hydrolysis in distilled water ($c_{NaOH} = 0$) does not seem to alter θ_a appreciably at higher temperatures but θ_r decreases when temperature increases to 60 °C. Which effect must result from a different "sensitiv-

Table 1. Coefficient of Determination and Parameters of the Sigmoid Function $y = a + b/\{1 + \exp[-(x - c)/d]\}$ Fitting the θ_a vs c_{NaOH} and γ_{SL} vs c_{NaOH} Dependences

T, °C	r^2	a	b	c	$-d$
		θ_a vs c_{NaOH}			
20	0.99868	63.965	14.061	5.085	0.961
40	0.99979	55.096	25.465	3.509	0.975
60	0.99999	50.678	36.767	1.809	1.046
		γ_{SL} vs c_{NaOH}			
20	0.96353/0.99839	18.415/16.887	8.210/11.203	4.158/4.628	0.078/0.480
40	0.99268/0.97234	12.500/11.516	18.446/18.408	2.944/2.970	0.681/0.678
60	0.95854/0.98827	4.017/4.744	33.281/29.719	1.799/1.908	0.716/0.324

ity" of the receding contact angle to surface characteristics of PET. However, the simultaneous rise of temperature and concentration of the NaOH pre-treatment solution has lead to a systematic decrease in θ_a as well as θ_r. Descending, S-shaped θ_a vs c_{NaOH} dependences are inferrable from Figure 6a with characteristic inflection points and horizontal asymptotes. Indeed, employing the TableCurve 2D curve fitting & equation discovery software it has been found that all dependences can be approximated with a very high fit goodness by the four-parameter sigmoid transition function $y = a + b/\{1 + \exp[-(x - c)/d]\}$ despite the limited number of experimental points.

It should be mentioned that the coefficient of determination r^2 in Table 1, whose value is quite high for all fits but may increase with increasing parameter counts, is comparable with the DOF adjusted r^2 coefficient of determination, accounting the number of parameters. (The approximation is used to represent the data for the purpose of extrapolation and interpolation, with the parameter count and values of secondary importance.)

It can be seen in Table 1 that the right-hand asymptote, i.e., the parameter a, predicts a lower limit of θ_a to be ca. 64, 55, and 50° for the 20, 40, and 60 °C curve, respectively. Correspondingly, the inflection point is predicted by the parameter c at ca. 5, 3.5, and 1.8% NaOH, respectively. It is noticeable that θ_a at these inflections is almost invariable (~70°).

To interpret the observed trends in the enhanced PET surface wettability, possible effects of side factors associated with the hydrolytic reaction at the PET surface should be examined. The problem is that the contact angle and its hysteresis on a surface is determined not only by its chemistry but also by an interplay of various nonidealities of the surface such as penetration, mobility, restructurization, swelling, dissolution, heterogeneity, and roughness (60). This consideration is not new, because the enhancement of surface wettability alone or combined with an altered pore distribution and connectivity and/or roughening has already been confirmed on hydrolyzed PET fibers, films, and fabric in order to improve their water retention and transport (absorbency) (33, 36, 61).

Therefore, let us ascertain whether some of the above enumerated surface alterations may concur in the collected contact angles and their hysteresis. It is almost certain that the pristine PET surface is chemically homogeneous (see also Figures 1a and 2a). It can be expected from the fact that the size of the repeated unit (the only surface heterogeneity) is only a few angstroms. This is too small to cause the hysteresis observed for the untreated PET.

It is also known that macromolecules with both hydrophilic and hydrophobic moieties at the surface of solid polymers in contact with water tend to restructure, i.e., to bury the hydrophobic (apolar) moieties and to expose the hydrophilic (polar) moieties to water (a polar medium); the opposite occurs in contact with air (an apolar medium), in order to minimize the interfacial free energy with the surrounding medium (62−64). Thus, it can be expected that the surface PET chains presenting a hydrophobic character in air may after restructuring display a less hydrophobic behavior in water and NaOH solutions.

The solid/water interfacial free energy drop $\Delta\gamma = \gamma_w(\cos\theta_a - \cos\theta_{a1}) = 13.4$ mJ m^{-2} of PET equilibrated with air (giving the static $\theta_{a1} = 81°$) and then dipped into water at ambient temperature to adjust its equilibrium conformations ($\theta_a = 70°$) was found to be comparable with the energy change $\Delta E_c = 8.6$ mJ m^{-2} (a result of molecular modeling) when the surface goes from the free state equivalent to a chain in air to the state where it is in contact with water (62). The correspondence of $\Delta\gamma$ with ΔE_c was suggested to confirm the assumption that the decrease of the advancing contact angle from θ_{a1} to θ_a can be solely due to the conformational restructuring of macromolecules at the amorphous PET surface. A coil-like structure of these macromolecules should dominate in air, favoring the PET-PET interactions, whereas more "stretched" conformations are preferred in water, tending toward the planar zig-zag structure and maximizing the hydrogen-bond formation with water molecules.

However, the time period required to change the system from the initial state to the final equilibrium state was very long (100 h) in (62) and since the values of advancing contact angles observed on untreated PET and PET immersed in water at 20 °C (for 20 min) were found to be almost identical, the molecular rearrangements are probably not influential enough in our study, at least for PET0/20. This also seems to be a true for the PET pretreated in water at higher temperatures because a slight increase in θ_a could be observed for PET0/20, PET0/40 and PET0/60 (see Figure 6a), despite of the fact that the relaxation time for the PET polymer surface to reorient and equilibrate itself have to

decrease dramatically at higher temperatures of water as also documented in ref 62.

Finally, it is known that chemical heterogeneity in conjunction with physical roughness, as in the case of textured PET surface because of the hydrolytic pretreatment, magnify wetting properties of solids in a complicated way (65). On the one hand, Wenzel's relation predicts the so-called apparent contact angle θ^* on chemically homogeneous surface to decrease with respect to the local or intrinsic (Young) contact angle θ_Y as the surface roughness is deepening, which is in qualitative agreement with the decrease in advancing and receding water contact angles on PET surfaces gradually roughened by hydrolysis up to 4% NaOH at 40 °C (see Figure 3). It cannot, however, explain the continuation in both these angles for surfaces hydrolyzed in 6% NaOH at the same temperature because the roughness is reverting.

On the other hand, the impact of nanometer-scale surface morphology on wetting was studied in ref 66, enabling us to parametrize the roughness factor r (Wenzel ratio defined as a ratio of the effective surface to the projected one). The result was that although the advancing and receding contact angles were found to correlate with the increasing r (1 to 1.07) the high values of the contact angle hysteresis (tens of degrees) could not be explained only by this factor. Some studies deal with a precise evaluation of the roughness factor (e.g., ref 67), from AFM scans of rough surfaces, but their results are also not conclusive enough as to the role of r (especially at the nanometer scale) in wetting.

In this situation, we can make a rough estimate as follows. Let us assume that the average contact angle $(\theta_a - \theta_r)/2 = 75°$ measured on the smooth, untreated PET surface is θ_Y and the limiting average contact angle on the PET surface immersed in 6% NaOH at 40 °C is θ^* due solely to the surface roughness imparted by the pretreatment (without the polarity modification). Then, according to the Wenzel equation $r = \cos\theta^*/\cos\theta_Y$, the value of r should be as high as 2.35. This value is much higher than that expected from S_a (4 nm at maximum at the scan size of $30 \times 30\ \mu m^2$) for PET6/40. This fact simply indicates that the surface nonidealties are not important in the establishment of contact angles on hydrolyzed PET surfaces under study.

In fact, it is well-known that the contact angle hysteresis increases with the surface roughness if the latter is above ca. 10 nm or so. The water contact angle hysteresis defined by eq 5 rises continually with the increasing NaOH concentration only at 20 °C, whereas an inverse trend is observed at 60 °C, with the intermediate one at 40 °C (Figure 6c).

3.6. Surface and Interfacial Energy. Two bicomponental wetting theories have been used by various authors to determine the apolar (dispersive) and polar (nondispersive) component of surface energy γ_S for PET by measuring advancing contact angles of test liquids on it. The apolar−polar approach has provided the dispersive and polar component $\gamma_S^d = 37.02$ mJ m^{-2} and $\gamma_S^P = 5.33$ mJ m^{-2}, respectively, so that $\gamma_S = \gamma_S^d + \gamma_S^P = 42.35$ mJ m^{-2} (55, 56). More data are available from studies rest on the LW-AB or VCG approach, yielding $\gamma_S^{LW} = 43.36$ mJ m^{-2}, $\gamma_S^+ = 0.003$ mJ m^{-2}, and $\gamma_S^- = 7.17$ mJ m^{-2} so that $\gamma_S^{AB} = \sqrt{\gamma_S^+\gamma_S^-} = 0.29$ mJ m^{-2} and thus $\gamma_S = \gamma_S^{LW} + \gamma_S^{AB} = 43.65$ mJ m^{-2} (68).

Using the latter approach with corrected acid−base parameters of water as a reference solvent and basing on the linear solvation energy relationship (LSER) of Taft or solvatochromic parameters (assuming that for water the ratio γ_L^+/γ_L^- is 1.8), the values $\gamma_S^{LW} = 43.50$ mJ m^{-2}, $\gamma_S^+ = 0$, $\gamma_S^- = 4.6$ mJ m^{-2}, $\gamma_S^{AB} = 0$, and $\gamma_S = 43.50$ mJ m^{-2} were obtained (69). Finally, the adoption of the same Taft acid−base scale with a "more realistic" ratio $\gamma_L^+/\gamma_L^- = 6.5$ for water (70), resulted in $\gamma_S^{LW} = 41.80$ mJ m^{-2}, $\gamma_S^+ = 0.0208$ mJ m^{-2}, $\gamma_S^- = 2.18$ mJ m^{-2}, $\gamma_S^{AB} = 0.43$ mJ m^{-2}, and $\gamma_S = 42.23$ mJ m^{-2}.

If the above values of surface energy determined by different authors and theoretical approaches for PET are averaged, the result is 42.93 mJ.m^{-2}, with the variation of only 1.42 mJ.m^{-2}, i.e., 3.3%. This looks as a good estimate, despite of different values of contact angles of test liquids measured and inserted in the calculations. For an illustration, the water contact angle on PET was 76.5, 77.1, 79.05, and 80.32° (in the presented order). Nevertheless, the polar or Lewis acid−base component of surface energy varies from 0 to 5.33 mJ m^{-2}, although the variation obtained merely with the VCG model is much lower (0−0.43 mJ m^{-2}).

The values of the LW and AB components of surface energy of the NaOH-pretreated PET surfaces calculated by solving of eq 6 for the BN-GL-W and DM-GL-W triplets of test liquids are summarized in Table 2 together with the experimental values of advancing contact angle averages of drops of these liquids taken in the calculation. It can be seen in Table 2 that the surface energy of PET immersed in distilled water at 20 °C is 43.28 mJ m^{-2}, if the DM-GL-W triplet is considered. This value is very close to the above-mentioned value of 42.93 mJ m^{-2}, obtained by averaging the data published up to now. Notice that the advancing contact angle of water droplets 78.2° lies in the middle of the published range (76.5 to 80.3°). The value 40.53 mJ m^{-2} provided by the B-G-W triplet seems to underestimate γ_S a little bit. Nonetheless, both triples give comparable γ_S's for the rest of PET surfaces.

More importantly, it can be observed in Table 2 that the total surface energy increases with both the NaOH concentration and temperature of the pretreatment solution, from $\gamma_S \approx 43$ mJ m^{-2} for untreated PET to $\gamma_S \approx 50$−51 mJ m^{-2} for PET pretreated in 6% NaOH at 40 °C. At the same time, it is noticeable that the increase in γ_S is partially due to a continuous increase of the LW component γ_S^{LW} from ca. 42 mJ m^{-2} to ca. 44 but mainly of the AB component γ_S^{AB} from ca. 1 mJ m^{-2} to ca. 7−8 mJ m^{-2}, mainly on account of the electron-donor parameter γ_S^- (data not shown here). Lower values of γ_S^{AB} (changing in a less systematic way) and, concomitantly, γ_S can be inferred from Table 2 for PET foils pretreated at 60 °C, although γ_S^{LW} continues to increase smoothly with the increasing NaOH concentration also at this pretreatment temperature. The reason of the above effect is probably a dramatic increase of dissolution of the

Table 2. Surface Energy Components of Modified PET, Calculated from Experimental Advancing Contact Angles of Two Different Triplets of Test Liquids (BN-GL-W/DM-GL-W)[a]

	θ_{BN} (deg)	θ_{DM} (deg)	θ_{GL} (deg)	θ_W (deg)	γ_S^{LW}(mJ m^{-2})	γ_S^{AB} (mJ m^{-2})	γ_S (mJ m^{-2})
			20 °C				
water only	28.15 ± 1.49	34.48 ± 0.46	71.71 ± 0.37	78.20 ± 0.56	39.30/42.26	1.23/1.02	40.53/43.28
2% NaOH	20.94 ± 1.47	33.74 ± 0.37	66.01 ± 0.71	77.15 ± 0.55	41.52/42.61	2.28/1.30	43.80/43.91
4% NaOH	20.55 ± 0.47	33.38 ± 0.49	63.14 ± 0.36	74.71 ± 0.66	41.62/42.76	3.24/2.15	44.86/44.91
6% NaOH	18.48 ± 0.62	31.19 ± 0.56	61.93 ± 0.52	67.82 ± 0.50	42.14/43.72	3.08/1.24	45.22/44.96
8% NaOH	5.65 ± 0.53	30.52 ± 0.34	55.54 ± 0.89	64.64 ± 0.76	44.18/44.01	6.09/4.09	50.27/48.10
			40 °C				
water only	17.21 ± 1.25	34.39 ± 0.46	69.85 ± 0.71	79.94 ± 1.16	42.44/42.31	1.03/0.20	43.47/42.51
2% NaOH	16.52 ± 0.04	33.56 ± 0.40	65.90 ± 0.84	75.99 ± 1.21	42.59/42.68	2.22/1.16	44.81/43.84
4% NaOH	16.25 ± 0.58	33.13 ± 0.48	59.09 ± 1.00	64.8 ± 1.29	42.64/42.88	4.24/3.25	46.88/46.13
6% NaOH	11.55 ± 0.37	31.06 ± 0.83	50.77 ± 1.16	56.71 ± 0.95	43.51/43.78	8.06/5.75	51.57/49.53
8% NaOH	6.08 ± 0.14	17.06 ± 0.24	46.03 ± 0.21	55.68 ± 0.93	44.15/48.59	10.37/5.89	54.52/54.48
			60 °C				
water only	15.03 ± 0.28	29.46 ± 0.51	66.64 ± 0.47	81.90 ± 0.73	42.90/44.44	2.17/0.19	45.07/44.63
2% NaOH	10.50 ± 0.42	26.77 ± 0.22	62.55 ± 0.79	67.39 ± 1.17	43.66/45.50	2.62/0.01	46.28/45.51
4% NaOH	7.79 ± 0.68	24.09 ± 0.14	60.98 ± 0.89	54.69 ± 1.23	43.99/46.47	4.10/0.41	48.09/46.88
6% NaOH	5.20 ± 0.28	21.59 ± 0.48	58.32 ± 0.33	51.40 ± 1.45	44.22/47.30	1.14/0.85	45.36/48.15
8% NaOH	2.91 ± 0.05	17.23 ± 0.11	47.47 ± 0.29	50.73 ± 1.11	44.34/48.55	9.44/4.28	53.78/52.83

[a] BN, $\gamma_L^{LW} = \gamma_L = 44.4$ mJ m^{-2}; DM, $\gamma_L^{LW} = \gamma_L = 50.8$ mJ m^{-2}; GL, $\gamma_L^{LW} = 34.0$ mJ m^{-2}, $\gamma_L^{+} = 3.92$ mJ m^{-2}, $\gamma_L^{-} = 57.4$ mJ m^{-2}, $\gamma_L^{AB} = 30.0$ mJ m^{-2}, $\gamma_L = 64.0$ mJ m^{-2}; W: $\gamma_L^{LW} = 21.8$ mJ m^{-2}, $\gamma_L^{+} = 25.5$ mJ m^{-2}, $\gamma_L^{-} = 25.5$ mJ m^{-2}, $\gamma_L^{AB} = 51.0$ mJ m^{-2}, $\gamma_L = 72.8$ mJ m^{-2}.

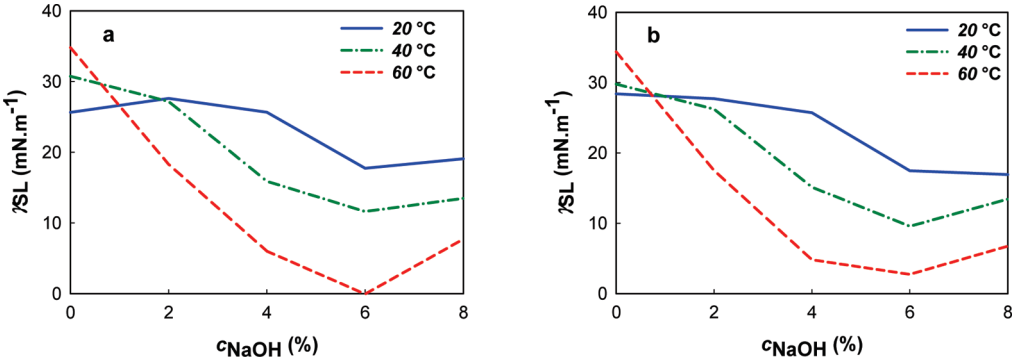

FIGURE 7. Interfacial tension of the PET/water interface as a function of concentration of the NaOH pretreatment solution, calculated from contact angle data of (a) BN-GL-W and (b) DM-GL-W triplets of test liquids.

PET surface, pretreated in NaOH solutions at 60 °C (reflecting fast dissolution during this pretreatment), in contact with polar but not apolar test liquids in the course of contact angle measurements. Additional measurements employing another polar test liquids would better specify the trends in γ_S^{AB}.

Panels a and b in Figure 7 display the interfacial free energy or tension γ_{SL} calculated for the PET surface in contact with water, depending on the concentration and temperature of the NaOH pretreatment solution, from the data given in Table 2 by applying eq 7. It can be seen in both figures that there is a decrease in the γ_{SL} from around 30 mJ m^{-2} to ~0 as the extent of hydrophilization of PET attains a maximum, being pretreated in 6% NaOH at 60 °C. Interestingly, as confirmed by the TableCurve software, all the γ_{SL} vs c_{NaOH} dependence maintain the sigmoidal course and inflections of the θ_a vs c_{NaOH} curves for water drops, although the fitting goodness is lower (see Table 1). Likewise, the values of γ_{SL} that correspond to the inflections vary within a narrow range (19.5−22.5 mJ m^{-2}).

It has been recognized earlier that there is a parallelism between solubility of a solid in liquids and the interfacial tension between the solid and liquids, γ_{SL}. In terms of chemical equilibrium, solubility is defined as the amount of a solute continually passing from the solid into saturated solution (dissolving) at the same rate as the solute is returning (crystallization) to the solid. Therefore, crystal growth, dissolution, and solubility are three important and mutually interconnected processes for a solid solute. The kinetics of the former two is influenced by thermodynamic driving forces. That is, low values of interfacial tension together with a high water surface tension facilitate dissolution of more hydrophilic solids in aqueous solutions whereas higher values of γ_{SL} cause a greater energy requirement for the dissolution of less-hydrophilic solids (71, 72).

Simultaneously, the dissolution process itself allows the interfacial tension to minimize, ultimately leading to $\gamma_{SL} \rightarrow 0$. The solid/water interfacial free energy γ_{SL} of the partially hydrophilic polymer films was found to decrease from an instantaneous value of ~50 mJ m^{-2} to an equilibrium value

of ~26.6 mJ m^{-2} over duration of 24 h (63, 64). However, films with an enhanced surface polarity (and roughness) manifested a much more dramatic decrease of the interfacial tension from 22 mJ.m^{-2} to a quasiequilibrium value of −1.6 mJ m^{-2} in a period of about 2 h. So, the decrease of γ_{SL} to a near-zero value because of a structure alteration was considered to stimulate a penetration of water into the films and their dissolution in water.

In traditional theories, it is assumed that dissolution, if initiated, continues spontaneously until all the solid phase has disappeared, i.e., when a true equilibrium has been reached. However, when the dissolution reaction is controlled by a formation and subsequent growth of pits (polypitting), it is only if a pit of certain size is reached that the dissolution may become spontaneous; simultaneously, the dissolution rate can be suppressed when pits become large enough to intersect each other, even though the solution remained undersaturated (73, 74). Apparently, there is a relationship between the dissolution rate and the size and number of pits.

We believe that the detected continuous decrease in γ_{SL} with increasing concentration of NaOH solution is a reflection of the primary tendency to minimize it through dissolution, with a "final" limit of $\gamma_{SL} = 0$ approached in 6 % NaOH at 60 °C. See especially the green line in Figure 7a. At the same time, the inflections of γ_{SL} vs c_{NaOH} curves at a nearly constant value of γ_{SL} but at different c_{NaOH} (depending on the temperature) may signalize a situation when the critical size of pits is attained, causing an attenuation of the ongoing dissolution process.

A specific feature of all curves, i.e., the increase in γ_{SL} for c_{NaOH} above 6 %, unlike the monotonously descending θ_a vs c_{NaOH} curves (Figure 6), can be ascribed to chemicrystallization of monomers extracted repeatedly and consecutively from the polymer chain ends at the PET surface (unzipping). Chemicrystallization of low-molecular-weight compounds extracted from the PET surface as a result of random chain scissions (a purely statistical process without any preferential sites of the chain, i.e. all bonds are equally probable toward hydrolysis) can also apply. Alternatively the increase in γ_{SL} for c_{NaOH} above 6 % may be an artifact, due to dissolution of PET surface during the contact angle measurements, which can be associated with its extreme dissolution in NaOH solutions of highest concentrations, especially at higher temperatures (see above).

4. CONCLUSIONS

On the basis of the measurement of advancing water contact angles, θ_a, the surface wettability of PET foils was found to be enhanced after immersing them in the NaOH pretreatment solution whose concentration, c_{NaOH}, increases from 0 to 8 %. The descending dependence of θ_a on c_{NaOH} is of sigmoidal character with an inflection point and a pronounced lower (right-hand) asymptotic wettability. The wettability of PET surfaces is further strengthened when temperature of the NaOH solution increases, as manifested by a proportional shift of the θ_a vs c_{NaOH} sigmoid with asymptotic $\theta_a = 64$, 55, and 50° and inflection at $c_{NaOH} = 5.0$, 3.5, and 1.8 % for the temperature equal to 20, 40, and 60 °C, respectively. This is accompanied with a convex−concave transition of the sigmoid's course and the inflection positioned at an unique value of $\theta_a \approx 70°$.

Analogously, dependences of the interfacial free energy, γ_{SL}, at the PET/water interface (calculated according to the surface thermodynamic LW-AB theory from θ_a of test liquid triplets) on c_{NaOH} obtained for the three temperatures maintain the sigmoidal shape with inflections at almost identical γ_{SL} (≈ 20 mJ m^{-2}) but displaced c_{NaOH}. A final limit of the PET surface hydrophilicity is prescribed thermodynamically as $\gamma_{SL} \rightarrow 0$, corresponding to θ_a of water about 50° on PET pretreated in 6 % NaOH at 60 °C.

Together with hydrophilicity, the surface roughness parameter, S_a, of PET foils pretreated in NaOH solutions at 40 °C also increases with the NaOH concentration. However, it reaches a maximum for $c_{NaOH} = 4$ % (PET4/40), which value is comparable with that detected at the inflection of the θ_a vs c_{NaOH} dependence. As the advancing contact angle and corresponding interfacial tension data are assumedly not influenced by the nanometer scale surface roughness, they should primarily reflect the chemistry of the NaOH-modified PET/water interface.

However, the surface roughness of PET surface due to the hydrolytic degradation may be at origin of the S shaped dependences of θ_a and γ_{SL} on c_{NaOH}. That is, on one hand, individual pits initially formed and grown on the PET surface, finding expression in increasing S_a, promote the hydrolytic reaction and associated dissolution of reaction products. On the other hand, when "critical" pits begin to connect each other, being reflected as a decrease in S_a, the accelerated dissolution reaction suddenly slows down.

The ζ potential evaluated by the electrokinetic (streaming current) measurements may also serve as a measure of the chain scissions and functional carboxyl and hydroxyl groups formed on the PET surface while hydrolyzably degrading even in the mildest conditions.

Acknowledgment. Financial support from the Scientific Grant Agency of the Slovak Republic (Project VEGA 2/0159/08) and from the Slovak Research and Development Agency (Project APVV-0598-07) is gratefully acknowledged.

REFERENCES AND NOTES

(1) Dodbiba, G.; Haruki, N.; Shibayama, A.; Miyazaki, T.; Fujita, T. *Int. J. Mineral Process.* **2002**, *65*, 11–29.
(2) Marques, G. A.; Tenorio, J. A. S. *Waste Manage.* **2000**, *20*, 265–269.
(3) Pongstabodee, S.; Kunachitpimol, N.; Damronglerd, S. *Waste Manage.* **2008**, *28*, 475–483.
(4) Pascoe, R. D.; O'Connell, B. *Waste Manage.* **2003**, *23*, 845–850.
(5) Okuda, T.; Kurose, K.; Nishijima, W.; Okada, M. *Ozone: Sci. Eng.* **2007**, *29*, 373–377.
(6) Reddy, M. S.; Kurose, K.; Okuda, T.; Nishijima, W.; Okada, M. *Resourc. Conserv. Recycl.* **2008**, *52*, 941–946.
(7) Reddy, M. S.; Kurose, K.; Okuda, T.; Nishijima, W.; Okada, M. *J. Hazard. Mater.* **2007**, *147*, 1051–1055.
(8) Ferreira, L.; Evangelista, M. B.; Martins, M. C. L.; Granja, P. L.; Esteves, J. L.; Barbosa, M. A. *Polymer* **2005**, *46*, 9840–9850.
(9) Kurose, K.; Okuda, T.; Nakai, S.; Tsai, T. Y.; Nishijima, W.; Okada, M. *Surf. Rev. Lett.* **2008**, *15*, 711–715.
(10) Wei, Q.; Liu, Y.; Hou, D.; Huang, F. *J. Mater. Process. Technol.* **2007**, *194*, 89–92.

(11) Katsikogianni, M.; Amanatides, E.; Mataras, D.; Missirlis, Y. F. *Colloids Surf., B* **2008**, *65*, 257–268.
(12) Rusu, I. A.; Popa, G.; Saied, S. O.; Sullivan, J. L. *J. Optoelectron. Adv. Mater.* **2006**, *8*, 1935–1938.
(13) Papakonstantinou, D.; Amanatides, E.; Mataras, D.; Ionnidis, V.; Nikolopoulos, P. *Plasma Process Polym.* **2007**, *4*, 1057–1062.
(14) Almazán-Almazán, M. C.; Paredes, J. I.; Pérez-Mendoza, M.; Domingo-Garcia, M.; López-Garzón, F. J.; Martínez-Alonso, A.; Tascón, J. M. D. *J. Colloid Interface Sci.* **2006**, *293*, 353–363.
(15) Yang, P.; Deng, J. Y.; Yang, W. T. *Polymer* **2003**, *44*, 7157–7164.
(16) Drelich, J.; Payne, T.; Kim, J. H.; Miller, J. D. *Polym. Eng. Sci.* **1998**, *38*, 1378–1386.
(17) Sisol, M. Flotation Separation of Plastics. MSc. Thesis., Technical Unversity in Košice, Košice, Slovak Republic, 2006; p 103 (in Slovak).
(18) Avadaneim, L.; Szilagyi, N. M.; Avadanei, V. *Mater. Plast.* **2002**, *39*, 234–239.
(19) Karayannidis, G. P.; Achilias, D. S. *Macromol. Mater. Eng.* **2007**, *292*, 128–146.
(20) Zenda, K.; Funazukuri, T. *J. Chem. Technol. Biotechnol.* **2008**, *83*, 1381–1386.
(21) Carta, D.; Cao, G.; D'Angeli, C. *Environ. Sci. Pollution Res.* **2003**, *10*, 390–394.
(22) Yang, Y.; Lu, Y. J.; Xu, Y. Y.; Xiang, H. W. *Prog. Chem.* **2001**, *13*, 65–72.
(23) Paszun, D.; Spychaj, T. *Ind. Eng. Chem. Res.* **1997**, *36*, 1373–1383.
(24) Nikles, D. E.; Farahat, M. S. *Macromol. Mater. Engineering* **2005**, *290*, 13–30.
(25) Mancini, S. D.; Zanin, M. *Polymer-Plastics Technol. Eng.* **2007**, *46*, 135–144.
(26) Lorenzetti, C.; Manaresi, P.; Berti, C.; Barbiroli, G. J. *Polym. Environm.* **2006**, *14*, 89–101.
(27) Kosmidis, V. A.; Achilias, D. S.; Karayannidis, G. P. *Macromol. Mater. Engn.* **2001**, *286*, 640–647.
(28) Polk, M.; Leboeuf, L.; Shah, M.; Won, C.-Y.; Hu, X.; Ding, W. *Polym.—Plast. Technol. Engn.* **1999**, *38*, 459–470.
(29) Pirzadeh, E.; Zadhoush, A.; Haghighat, M. *J. Appl. Polym. Sci.* **2007**, *106*, 1544–1549.
(30) Hosseini, S. S.; Taheri, S.; Zadhoush, A.; Mehrabani-Zeinabad, A. *J. Appl. Polym. Sci.* **2005**, *103*, 2304–2309.
(31) Launay, A.; Thominette, F.; Verdu, J. *Polym. Degrad. Stab.* **1994**, *46*, 319–324.
(32) Golike, R. C.; Lasoski, S. W., Jr. *J. Phys. Chem.* **1960**, *64*, 895–898.
(33) Holmes, S. A.; Zeronian, S. H. *J. Macromol. Sci., Part A: Pure Appl. Chem.* **1994**, *A31*, 1147–1168.
(34) Holmes, S. A.; Zeronian, S. H. *J. Appl. Polym. Sci.* **1995**, *55*, 1573–1581.
(35) Sanders, E. M.; Zeronian, S. H. *J. Appl. Polym. Sci.* **1982**, *27*, 4477–4491.
(36) Zeronian, S. H.; Wang, H. Z.; Alger, K. W. *J. Appl. Polym. Sci.* **1990**, *41*, 527–534.
(37) Langevin, D.; Grenet, J.; Saiter, J. M. *Eur. Polym. J.* **1994**, *30*, 339–345.
(38) Sammon, C.; Yarwood, J.; Everall, N. *Polymer* **2000**, *41*, 2521–2534.
(39) Sammon, C.; Mura, C.; Yarwood, J.; Everall, N.; Swart, R.; Hodge, D. *J. Phys. Chem.* **1998**, *102*, 3402–3411.
(40) Kloppers, M. J.; Bellucci, F.; Lantanision, R. M.; Brennen, J. E. *J. Appl. Polym. Sci.* **1993**, *48*, 2197.
(41) Jacobasch, H. J. *Angew. Makromol. Chem.* **1984**, *128*, 47–69.
(42) Grundke, K.; Boerner, M.; Jacobasch, H. J. *Colloids Surf.* **1991**, *58*, 47–59.
(43) Bismarck, A.; Kumru, M. E.; Springer, J. *J. Colloid Interface Sci.* **1999**, *217*, 377–387.
(44) Kanamaru, K. *Koll. Z.* **1960**, *168*, 115–121.
(45) Temmel, S.; Kern, W.; Luxbacher, T. *Prog. Colloid Polym. Sci.* **2006**, *132*, 54–61.
(46) Zembala, M. *Adv. Colloid Interface Sci.* **2004**, *112*, 59–92.
(47) Wunderlich, R. W. *J. Colloid Interface Sci.* **1982**, *88*, 385.
(48) Škvarla, J. *Langmuir* **2007**, *23*, 5305–5314.
(49) Saville, D. A. *J. Colloid Interface Sci.* **2000**, *222*, 137.
(50) Hayes, R. A. *Colloids Surf., A* **1999**, *146*, 89–94.
(51) Schnitzer, Ch.; Ripperger, S. *Chem. Eng. Technol.* **2008**, *31*, 1696–1700.
(52) Ramsden, M. J.; Phillips, J. A. *J. Chem. Technol. Biotechnol.* **1996**, *67*, 131–136.
(53) Voigt, A.; Wolf, H.; Lauckner, S.; Neumann, G.; Becker, R.; Richter, L. *Biomaterials* **1983**, *4*, 299–304.
(54) Luxbacher, T. *Desalination* **2006**, *199*, 376–377.
(55) Jańczuk, B.; Białopiotrowicz, T. *J. Colloid Interface Sci.* **1989**, *127*, 189–204.
(56) Jańczuk, B.; Białopiotrowicz, T.; Wójcik, W. *J. Colloid Interface Sci.* **1989**, *127*, 59–66.
(57) Li, D.; Neumann, A. W. *J. Colloid Interface Sci.* **1992**, *148*, 190–200.
(58) Kwok, D. Y.; Neumann, A. W. *Colloids Surf., A* **2000**, *161*, 49–62.
(59) Wei, Q.; Tao, D.; Du, Z.; Cai, Y.; Wu, N.; Chen, L. *J. Appl. Polym. Sci.* **2008**, *109*, 654–658.
(60) Li, D.; Neumann, A. W. *J. Colloid Interface Sci.* **1990**, *137*, 304–307.
(61) Chong, E. K.; Stevens, M. G.; Nissen, K. E. *J. Adhes.* **2003**, *79*, 667–681.
(62) Vergelati, C.; Perwuelz, A.; Vovelle, L.; Romero, M. A.; Holl, Y. *Polymer* **1994**, *35*, 262–270.
(63) Ruckenstein, E.; Gourisankar, S. V. *J. Colloid Interface Sci.* **1985**, *107* (2), 488–502.
(64) Ruckenstein, E.; Gourisankar, S. V. *J. Colloid Interface Sci.* **1986**, *109* (2), 557–566.
(65) deGennes, P. G.; Brochard, Wyart.; Quéré, D. In *Capillarity and Wetting Phenomena. Drops, Bubbles, Pearls, Waves*; Springer: New York, 2004; p 287.
(66) Müller, B.; Riedel, M.; Michel, R.; De Paul, S. M.; Hofer, R.; Heger, D.; Grützmacher, D. *J. Vac. Sci. Technol., B* **2001**, *19*, 1715–1720.
(67) Kamusewitz, H.; Possart, W.; Paul, D. *Colloids Surf., A* **1999**, *156*, 271–279.
(68) Wu, W.; Giese, R. F., Jr.; van Oss, C. J. *Langmuir* **1995**, *11*, 379–382.
(69) Lee, L. H. *Langmuir* **1996**, *12*, 1681–1687.
(70) Della Volpe, C.; Siboni, S. *J. Adhesion Sci. Technol.* **2000**, *14*, 235–272.
(71) Wu, W.; Nancollas, G. H. *Advan. Colloid Interface Sci.* **1999**, *79*, 229–279.
(72) Wu, W.; Nancollas, G. H. *Pure. Appl. Chem.* **1998**, *70*, 1867–1872.
(73) Tang, R.; Orme, Ch. A. *J. Am. Chem. Soc.* **2001**, *123*, 5437–5443.
(74) Tang, R.; Noncollas, G. H. *Pure. Appl. Chem.* **2002**, *74*, 1851–1857.

AM100368V